High Resolution SAR Imaging and Signal Processing

Paulo A.C. Marques
Instituto Superior de Engenharia de Lisboa / Instituto de Telecomunicações
ISEL-ADEETC – R. Conselheiro Emidio Navarro, 1, Lisboa
PORTUGAL

pmarques@isel.pt

ABSTRACT

Synthetic aperture radar (SAR) is an active microwave system typically carried by an aircraft or a satellite that is able to produce high resolution images of a target area. This paper presents the basic principles of SAR imaging from a signal processing perspective, starting from an approximation for the received phase signal, for the sake of simplicity. It then introduces the wavefront image reconstruction algorithm which takes into consideration the exact phase history of the received signal. Other SAR imaging algorithms and imaging modes are also addressed.

1.0 INTRODUCTION

Ground surveillance radar is a useful tool for remote sensing. Airborne and spaceborne radar sensors are able to quickly cover large areas of the ground and to produce high quality radar maps, in all weather, day and night, see [1], [2].

The so-called strip-map SAR acquisition geometry, illustrated in Figure 1, is the most widely used. This acquisition geometry provides data along a terrain strip parallel to the flight direction (azimuth or cross-range direction). The radar travels at constant velocity in the azimuth direction and transmits wide-band microwave pulses at regular intervals. The corresponding echoes are recorded. Many pulses are transmitted during the so called integration time, i.e., the time the platform takes to travel the footprint cross-range length.

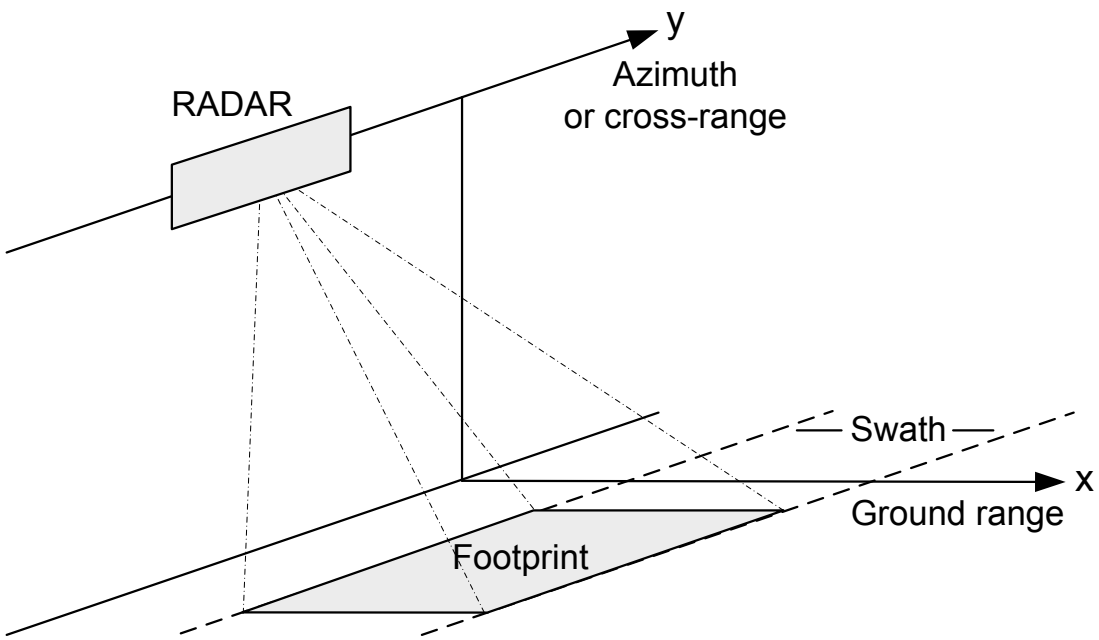

Figure 1: Strip-Map SAR Geometry.

High resolution in range is obtained using traditional pulse compression techniques and is independent of the antenna size (see, e.g., [2] Ch. 7]). Typical look angle values ranges from 20° to 60°. Small look angles lead to degradation of the ground range resolution, while large look angles produce strong shadow effects. High resolution in the azimuth direction is obtained via synthesizing a long array by taking advantage of the platform movement.

The paper is organized as follows.

Section 2 is dedicated to strip-map SAR imaging. It starts by presenting a comparatively simplified SAR imaging algorithm, which considers the range and cross-range domains as separable. The basic principle consists in implementing two-dimensional matched filtering. This algorithm, although an approximation, permits the focusing of SAR images with quality good enough for many applications.

It then proceeds with the wavefront reconstruction algorithm, which exploits the structure of the SAR signals in the Fourier domain. This algorithm tackles very accurately and efficiently the SAR inversion problem. It permits very high resolution imaging even in spaceborne applications. For a comprehensive treatment, see [3]. This section finishes with a briefly description of other popular SAR imaging algorithms.

Section 3 is dedicated to the SAR imaging modes. In this section, besides the strip-map SAR imaging, other imaging modes supported by more recent SAR systems are addressed.

Section 4 presents the final remarks.

2.0 SAR IMAGE FORMATION

2.1 SAR Imaging Considering Separable Range and Cross-Range Domains

For the sake of simplicity we will now consider separately range and cross-range processing. For this approach to hold, it is assumed that the distance from the RADAR platform to the target area is much larger than the antenna footprint in cross-range dimension.

2.1.1 Range Domain: Pulse Compression

A radar signal should permit to determine the range of a target and to distinguish it from others in its neighbourhood. Such a signal should have very short range extent and be powerful enough to maintain the necessary signal to noise ratio on the receiver. In theory, a signal such as $\delta(t)$ would conform to such specifications. However this kind of signal is not practical since it demands very short pulse duration with power enough to conform to SNR requirements. In practice, to obtain high resolution in the range direction, SAR systems typically transmit an alternative kind of signal, i.e. chirp signals which, basically, are frequency modulated waveforms. The basic idea is to transmit a relatively long pulse that has a bandwidth corresponding to a short duration pulse.

Let us consider the *chirp* waveform with duration T_p and bandwidth $\beta = \alpha T$, modulated in frequency, with constant amplitude:

$$s(t) = e^{j\alpha t^2} \tag{1}$$

As shown in [4] the emitted pulse can be compressed on the reception by correlating the received signal with a copy of the emitted pulse. The obtained resolution is given by:

$$\Delta x = \frac{c}{2\alpha T_p}. \tag{2}$$

Therefore, larger pulse duration achieves better range resolution.

Figure 2 illustrates qualitatively the pulse compression technique. The simulation considers five point-like targets at coordinates 30m, 70m, 100m, 130m, and 160m. Fig. 2 on top-left, shows the real part of the emitted chirp in baseband; on top-right, illustrates the five simulated targets and their relative reflectivity at the corresponding ranges; bottom-left, shows the received signal before pulse compression. As expected the several target echoes overlap and their relative reflectivities and positions are not resolvable. Fig. 2, bottom-right, shows the resulting signal after correlating with the emitted chirp. The *pulse compression* operation permits the detection of five targets and the estimation of their relative reflectivities.

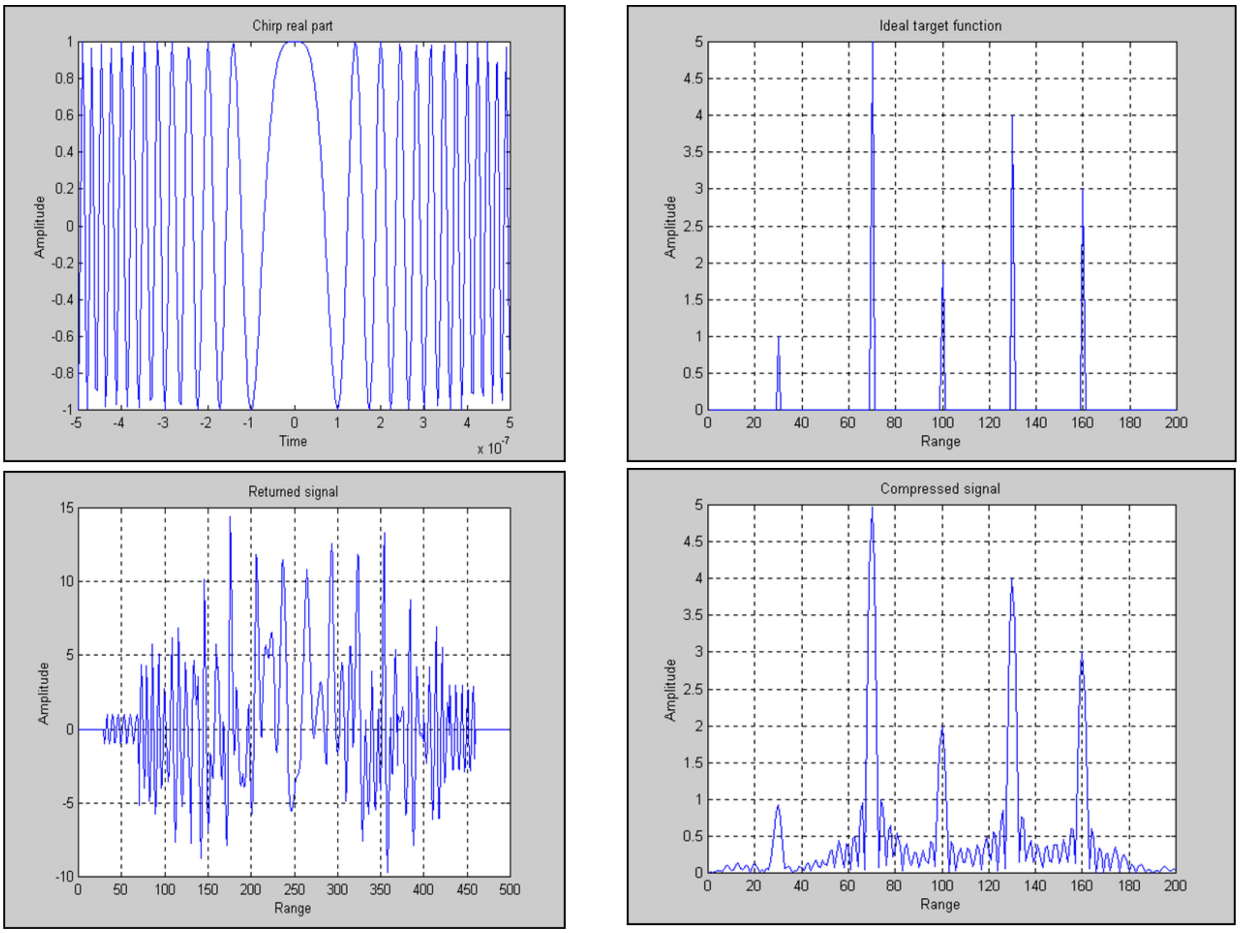

Figure 2: Pulse Compression Illustration.

2.1.2 Cross-Range Domain

For the sake of simplicity we will now analyse the SAR processing on the cross-range (or azimuth) direction, decoupled from the range axis.

Let us consider the scenario present in Figure 3 where the radar illuminates a single target while travelling along the azimuth direction. The received signal phase difference between the emitted and the echoed signals due to such a target is:

$$\Delta\theta = 2\pi f t_D, \tag{3}$$

where:

$$t_D = \frac{2R(y)}{c}, \tag{4}$$

and:

$$y = v_R t, \tag{5}$$

with:

$$c = f\lambda. \tag{6}$$

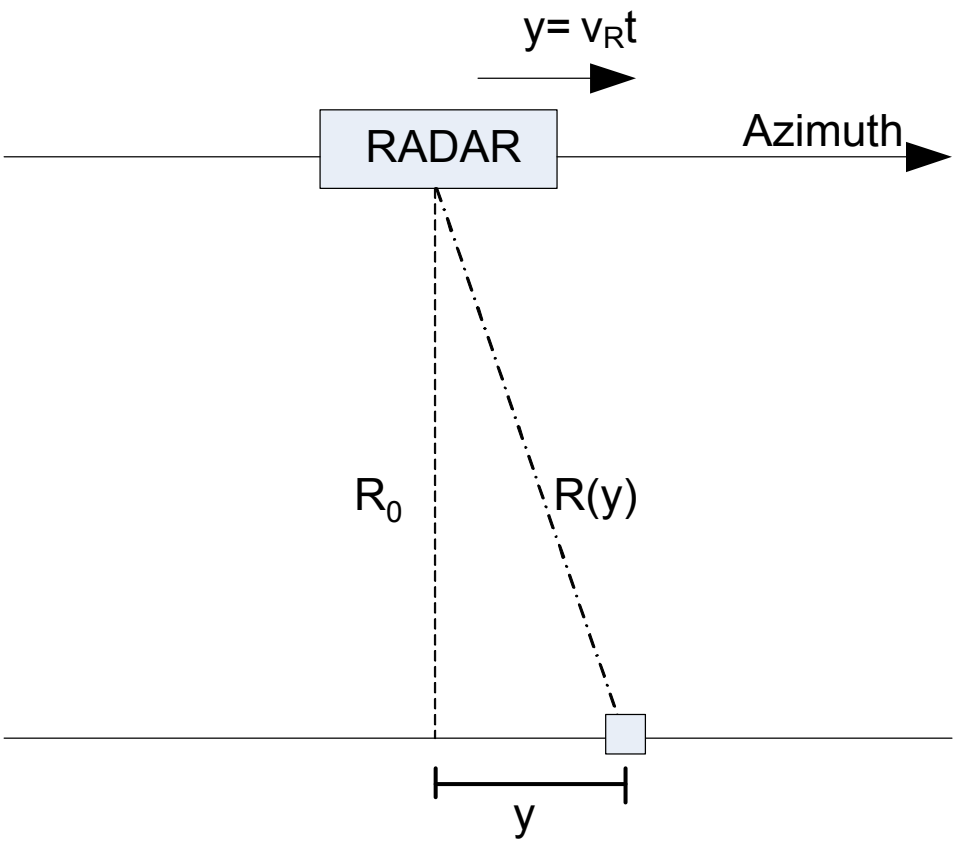

Figure 3: Azimuth Direction SAR Geometry.

By considering $R_0 \gg y$ the received signal phase difference can be approximated to:

$$\Delta\theta \approx \frac{4\pi R_0}{\lambda} + \frac{2\pi y^2}{2R_0}, \tag{7}$$

where R_0 denotes the closest approach distance between the radar and the target.

Therefore, the received signal can be written as:

$$s(y) \approx e^{j4\pi R_0/\lambda} e^{j2\pi y^2/\lambda R_0}, \tag{8}$$

where the second term is easily recognized as a *chirp*. Notice that this chirp, although due to the SAR geometry, can be also compressed using the correlation operation as happens with the emitted pulse in the range direction.

The azimuth resolution can be shown to be given by [4]:

$$\Delta y = D/2, \tag{9}$$

where D is the antenna length.

Therefore, smaller antenna leads to better resolution, in contrast to what would be achieved without any processing.

A very important aspect of SAR is the sampling in the cross-range direction. According to Shannon's sampling theorem, the signal should be larger than the bandwidth of the *cross-range chirp*. Therefore, the pulse repetition frequency (PRF) should obey to:

$$PRF \geq \frac{2v_R}{D}, \tag{10}$$

where v_R is the SAR platform velocity in the azimuth direction.

When range and cross-range directions can be decoupled it is possible to apply a simple SAR processor for focusing the raw-data as illustrated in Figure 4 for strip-map geometry.

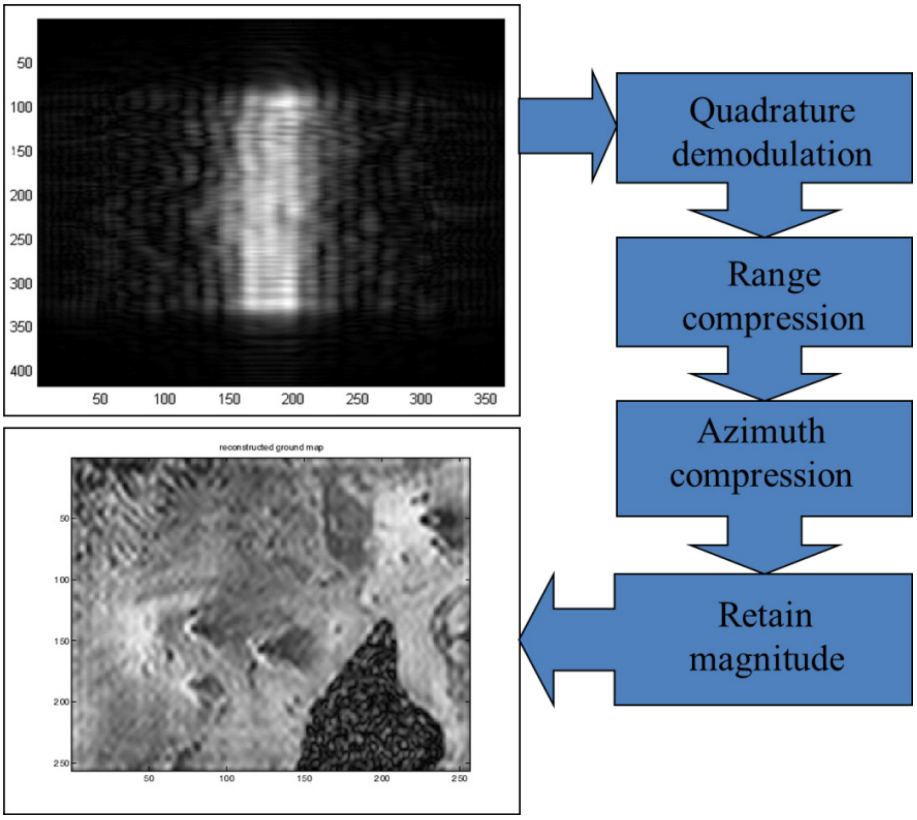

Figure 4: Simplified SAR Processor for Strip-Map Geometry. The range compressed data is obtained by a convolution with the range reference *chirp*; the azimuth compressed data is obtained by a convolution with the azimuth reference function.

Let us recall that without any processing the cross range resolution would be:

$$\Delta y = \frac{\lambda}{D} R_0. \tag{11}$$

That is, the resolution degrades with the range of the target. After processing, the obtained resolution is independent of the target area range and is given by:

$$\Delta y = \frac{D}{2}. \tag{12}$$

As a numerical example of the resolution enhancement gain by using SAR let us look at the parameters of the European Remote Sensing (ERS-1) satellite detailed on Table 1.

Table 1: ERS-1 Parameters.

Parameter	Value
Wavelength	$\lambda = 5.6cm$
Pulse bandwidth	$B = 15MHz$
Antenna size (in azimuth)	$D = 10m$
Look angle	$\theta = 23°$
Range	$R = 850km$

By using eq. (11) one can calculate a cross-range resolution of 4.8km. However, by using the motion of the antenna to synthesize a larger aperture, Eq. (12), the cross-range resolution becomes approximately 5m, i.e. a thousand times better!

2.2 Wavefront Reconstruction Algorithm

The algorithm presented in previous subsection is able to obtain SAR images with quality good enough for many applications. It uses a simple approach based on the validity of the quadratic approximation on the phase of the received signal. Under this assumption both dimensions can be processed separately.

For high accuracy SAR processing, however, one needs to take into consideration the exact phase history of the received signal. In this context we will now present the so-called wavefront reconstruction algorithm which exploits the structure of the SAR signals in the Fourier domain. This algorithm tackles very accurately and efficiently the SAR inversion problem even when the quadratic approximation is not valid.

This subsection follows very closely [3], [5] and [6].

Figure 5 shows a strip-map synthetic aperture radar scenario in the plane defined by the cross-range and the slant-range axes. Let us consider a radar platform moving with velocity v_R along a line known as the synthetic aperture domain or the cross-range domain. For a fixed platform position, $y = v_R t \equiv u$, the radar transmits a wide-band pulse $p(t)$, where t is the fast-time domain, and echoed signal from the illuminated area is recorded.

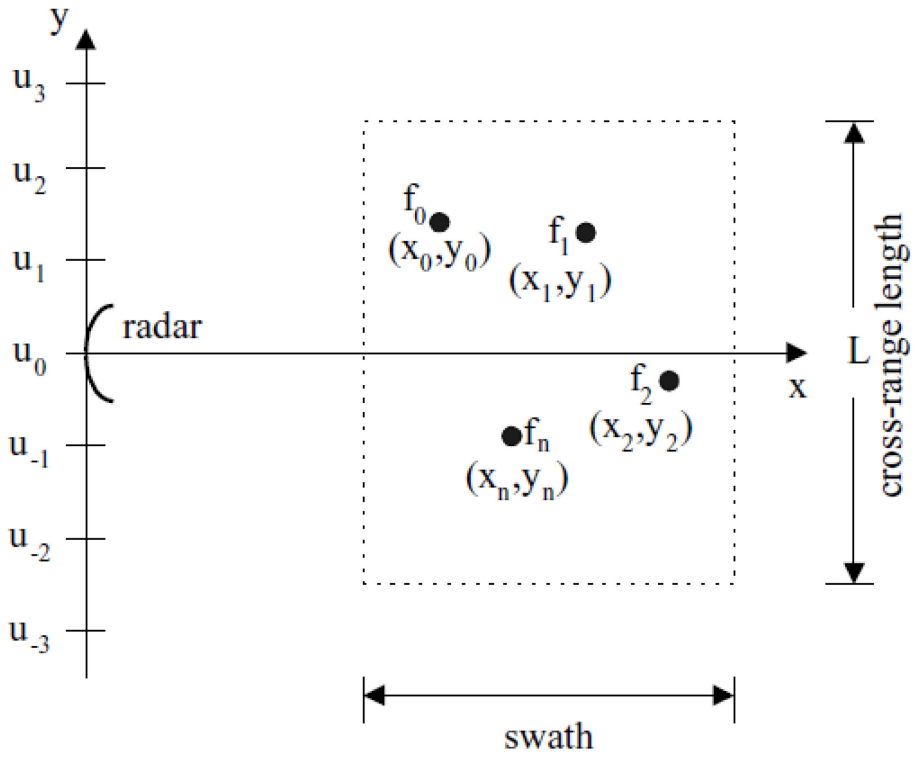

Figure 5: Considered SAR Scenario for 2-D Imaging with the Wavefront Algorithm.

Let us consider a target region composed of *N* static point-like targets with complex reflectivity f_n, where $n = 0, \dots, N-1$, and coordinates (x_n, y_n) as illustrated in Fig. 5.

The *target function* corresponding to this scenario is:

$$f(x,y) \equiv \sum_{n=0}^{N-1} f_n \delta(x - x_n, y - y_n). \tag{13}$$

The corresponding 2-D Fourier transform is:

$$F(k_x, k_y) = \sum_{n=0}^{N-1} f_n e^{-jk_x x_n} e^{-jk_y y_n}, \tag{14}$$

where k_x and k_y denote the spatial frequency with respect to coordinate *x* and *y*, respectively.

Radar imaging aims at determining the target function. To achieve this goal, we start by looking at the signal received by the radar.

The echoed signal when the platform is at position *y=u*, in the fast-time frequency domain and in the slow-time spatial domain:

$$s(\omega, u) = P(\omega) \sum_{n=0}^{N-1} a(\omega, y_n - u) f_n e^{-j2kr_n}, \tag{15}$$

where $P(\omega)$ is the low-pass equivalent Fourier transform of the emitted pulse $p(t)$, $a(\omega,u)$ is the low-pass equivalent of the two-way antenna radiation pattern in the (ω,u) domain, assumed to be independent of the slant-range coordinate x, $k \equiv (\omega+\omega_0)/c$ is the wavenumber, $f_0 = \omega_0/(2\pi)$ is the carrier frequency, and c is the speed of light. Symbol f_n denotes the complex reflectivity of the n*th* target, assumed to be independent of the aspect angle. Wave divergence is absorbed by f_n. Symbol r_n denotes the distance between the radar and the *nth* target and is given by:

$$r_n = \sqrt{x_n^2 + (y_n - u)^2}. \tag{16}$$

In [3] it is shown that the Fourier transform of $s(\omega,u)$, with respect to the slow-time domain, is:

$$S(\omega,k_u) = A(\omega,k_u)P(\omega)\sum_{n=0}^{N-1} f_n e^{-j\sqrt{4k^2-k_u^2}x_n} e^{-jk_u y_n}, \tag{17}$$

where $A(\omega,k_u)$ is the two-way antenna radiation pattern in the 2D frequency domain.

Comparing (14) with (17), we can write:

$$S(\omega,k_u)P(\omega)F(k_x,k_y), \tag{18}$$

where:

$$k_x \equiv \sqrt{4k^2 - k_u^2}, \tag{19}$$

and:

$$k_y \equiv k_u. \tag{20}$$

To estimate the target function, we adopt a matched filtering approach, which is the most frequently used in SAR applications, as it is light from the computational point of view and robust to model mismatches.

The output of the matched filter is thus:

$$\hat{F}(k_x,k_y) = A^*(k_x,k_y)P^*(k_x,k_y)S(k_x,k_y), \tag{21}$$

resulting:

$$\hat{F}(k_x,k_y) = |A(k_x,k_y)|^2 |P(k_x,k_y)|^2 \sum_{n=0}^{N-1} f_n e^{-jk_x x_n} e^{-jk_y y_n}. \tag{22}$$

In the spatial domain, we have:

$$\hat{f}(x,y) = \sum_{n=0}^{N-1} f_n h(x-x_n, y-y_n), \tag{23}$$

where $h(x,y)$ denotes the SAR system transfer function:

$$h(x,u) = FT^{-1}_{(x,u)}\left[\left|A(k_x,k_y)\right|^2\left|P(k_x,k_y)\right|^2\right]. \quad (24)$$

The wavefront reconstruction algorithm block diagram is presented in Figure 6 and is summarized by the following step sequence:

1) Compute $S(\omega,k_u)$, the two-dimensional Fourier transform of the received signal $s(t,u)$.
2) Implement the matched filtering in the frequency domain, by multiplying $S(\omega,k_u)$ with $S_0^*(\omega,k_u) = A^*(\omega,k_u)P^*(\omega)$.
3) Implement the change of variables (19) and (20), the so-called Stolt interpolation [12].
4) Calculate the two-dimensional inverse Fourier transform (22), obtaining $\hat{f}(x,y)$, the estimate of the target function.

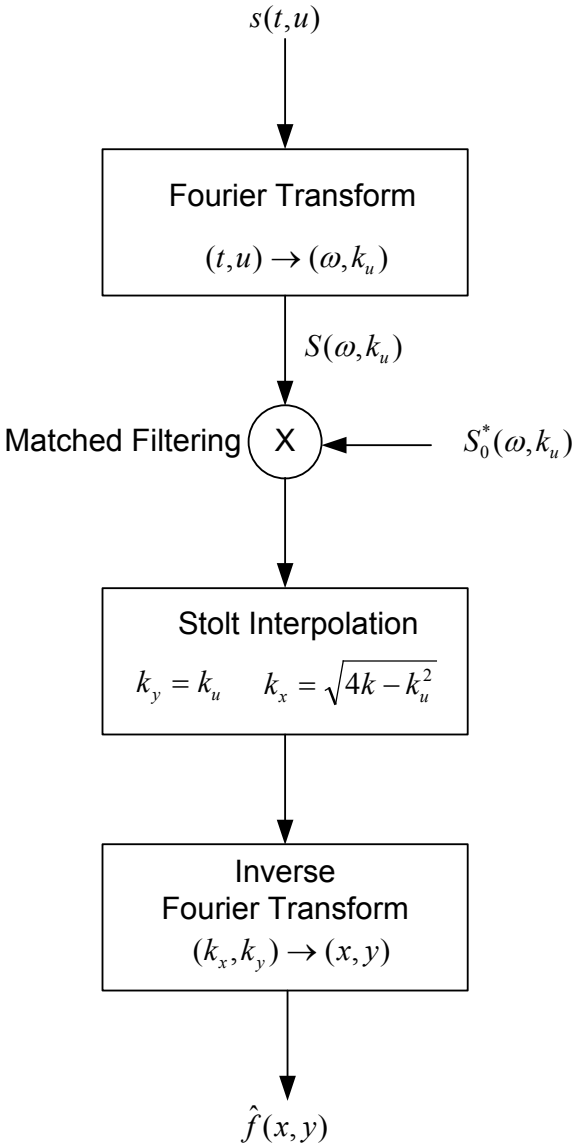

Figure 6: Wavefront Reconstruction Imaging Algorithm.

This imaging algorithm belongs to a class of algorithms often referred to as wavenumber domain or $\omega - k$ processors. This kind of processors is not new and has been used to perform seismic signal processing for imaging the substrata of Earth [7]. These ideas were later applied to imaging of SAR data [11].

2.3 Other SAR Imaging Algorithms

Most SAR imaging algorithms usually include three major steps:

- Range compression;
- Range cell migration compensation;
- Azimuth compression.

In the wavefront reconstruction algorithm just described, the range compression and (partial) azimuth compression are done in step 2. The range cell migration compensation is dealt with in step 3, where the Stolt interpolation decouples the spatial domains *x* and *y*.

A large number of SAR focusing algorithms, besides the wavefront reconstruction algorithm, have been presented in the literature. To reduce the computational requirements, at expense of image quality, some of the algorithms implement approximated range migration compensation or they do not implement it at all.

Herein we just present a brief summary of the three most popular focusing algorithms, besides the wavefront reconstruction already presented, for strip-map SAR.

2.3.1 Range-Doppler Algorithm

This algorithm is probably the most well-known SAR focusing scheme [1]. It starts with the 1-D transform of $s(t,u)$ to $s(t,k_u)$. The coupling between the range (time) and k_u is removed by a coordinate remapping via interpolation. The azimuth compression is then applied in the k_u domain. A single compression in the range-Doppler domain for each range is then applied to all pixels at the same range. In systems where range cell migration is small, the Fresnel approximation can be used without degrading too much the image quality and the interpolation step can be ignored (see, e.g., [8]).

2.3.2 Chirp-Scaling Algorithm

The chirp-scaling algorithm starts with the raw-echo data (without range pulse compression) because it exploits the linear FM (LFM) signal structure of the transmitted pulse [9]. If coded or pseudorandom sequences are used for the transmitted pulse, data must be range compressed with an adequate matched filter and then respread by a convolution with a LFM pulse. As in the range-Doppler approach, the algorithm starts with a 1-D transform in the slow-time domain of $s(t,u)$to $s(t,k_u)$. Then $s(t,k_u)$ is multiplied by a phase-only chirp which scales the range chirp for each k_u and t so that the Doppler *loci* of all targets end up with a common range migration in phase. The scaled data is then Fourier-transformed to (ω,k_u) domain, where range compression and range cell migration compensation are performed. Azimuth compression and residual phase compensation are then implemented in the (t,k_u) domain.

2.3.3 Time Domain Correlation Algorithm

The basic principle behind the time domain correlation (TDC) imaging algorithm is simply the implementation of the matched filtering via a two-dimensional correlation ([3], Ch. 4.7), similarly to algorithm presented in subsection 2.1. To reduce the numerical errors the signal is up-sampled (interpolated).

The major drawback of this algorithm is the high computational cost due to the brute force approach.

3.0 SAR IMAGING MODES

Besides the more fundamental strip-map imaging mode which has been previously presented, there are many others supported by the recent SAR systems. In order to support these imaging modes the antenna is divided into several sub-apertures. By controlling the phase and amplitude of each subaperture it is possible to change the antenna radiation pattern and, consequently, the illuminated region.

3.1 Strip-Map SAR

The strip-map SAR, which has been addressed in the previous sections, is the most common configuration. In this imaging mode the antenna patterns remains fixed and it illuminates a fixed swath. The data acquisition occurs for a continuous strip of the terrain as presented in Figure 7.

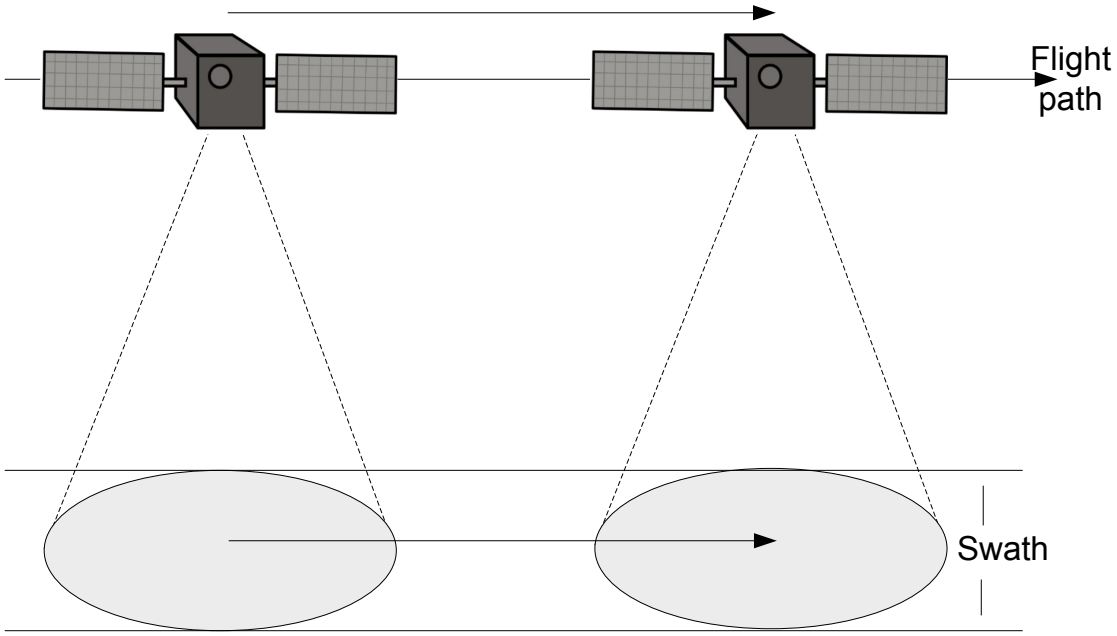

Figure 7: Strip-Map SAR Imaging Mode.

3.2 ScanSAR

The ScanSAR imaging mode is used when a wider swath is required. The antenna pattern is steered in elevation during the data acquisition interval. This leads to the illumination of several sub-swaths as illustrated in Figure 8. Since each sub-swath is illuminated during a fraction of time when compared with the strip-map situation, the azimuth resolution is proportionally degraded.

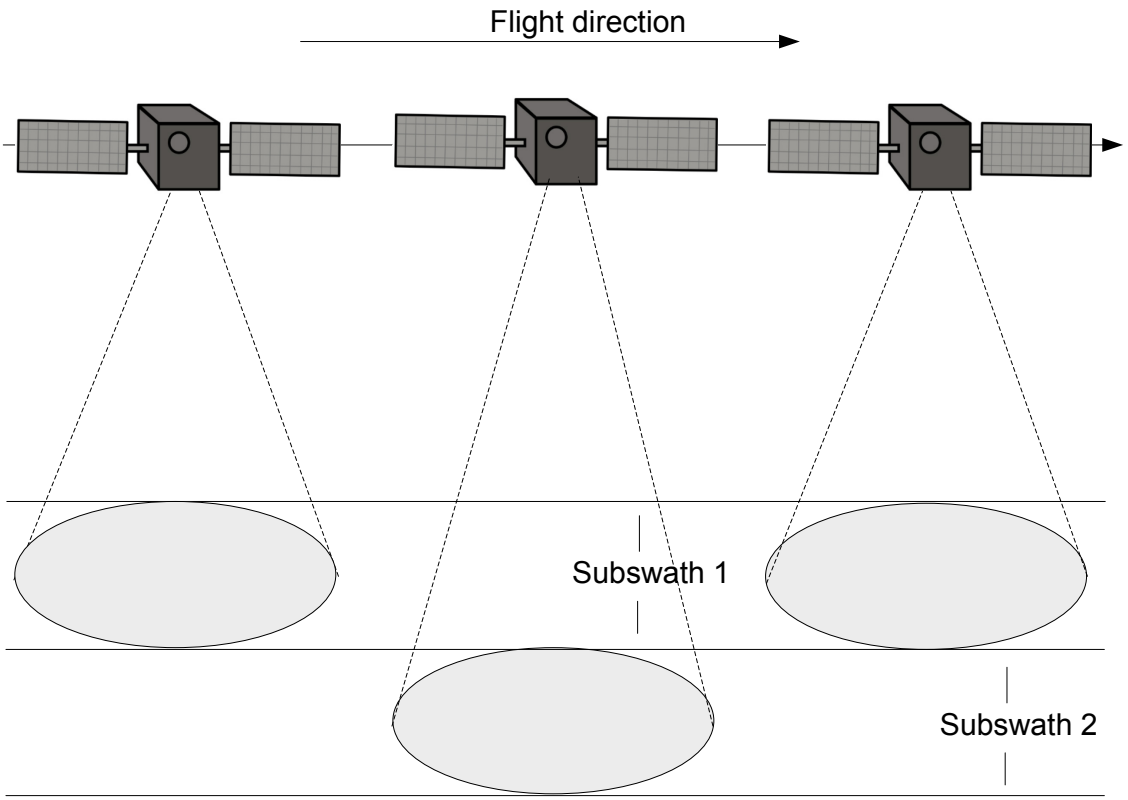

Figure 8: ScanSAR Mode Increases the Swath Width at Expenses of Azimuth Resolution.

3.3 Spotlight SAR

The spotlight SAR imaging configuration is used to obtain the best resolution of a certain target area. The resolution is enhanced by increasing the integration time. Figure 9 illustrates this imaging mode. The antenna pattern is steered in order to illuminate a fixed region of interest during a much longer interval than the one achieved in strip-map SAR operation. The increase in resolution is obtained at the cost of not imaging a continuous swath along the flight path.

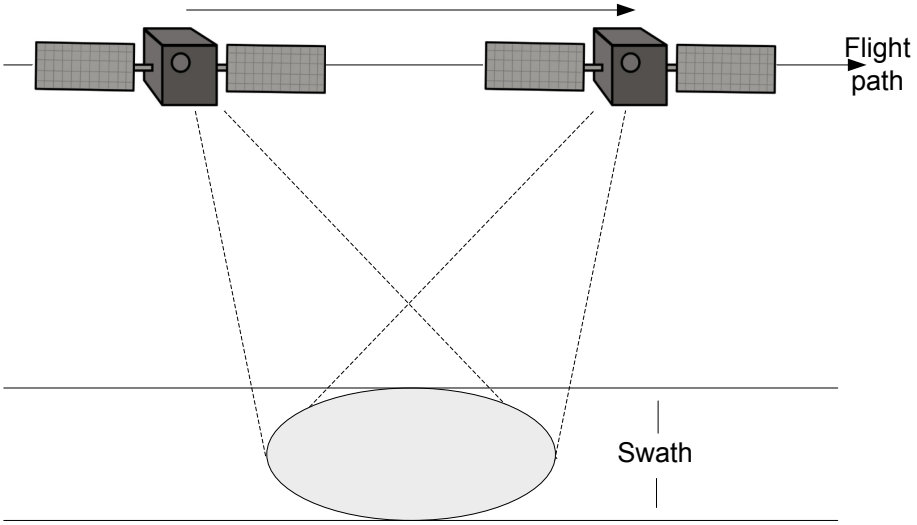

Figure 9: Spotlight Mode: Increases the Azimuth Resolution Having as Trade-Off the Decrease of the Swath Length.

3.4 High-Resolution Wide-Swath Imaging

To overcome the trade-off limitation between resolution in azimuth versus spatial coverage, a novel imaging technique has been proposed [10]. This imaging mode combines digital beamforming on receive in elevation with multiple aperture recording in azimuth. This strategy enables the imaging of wide swath while simultaneously obtaining high resolution.

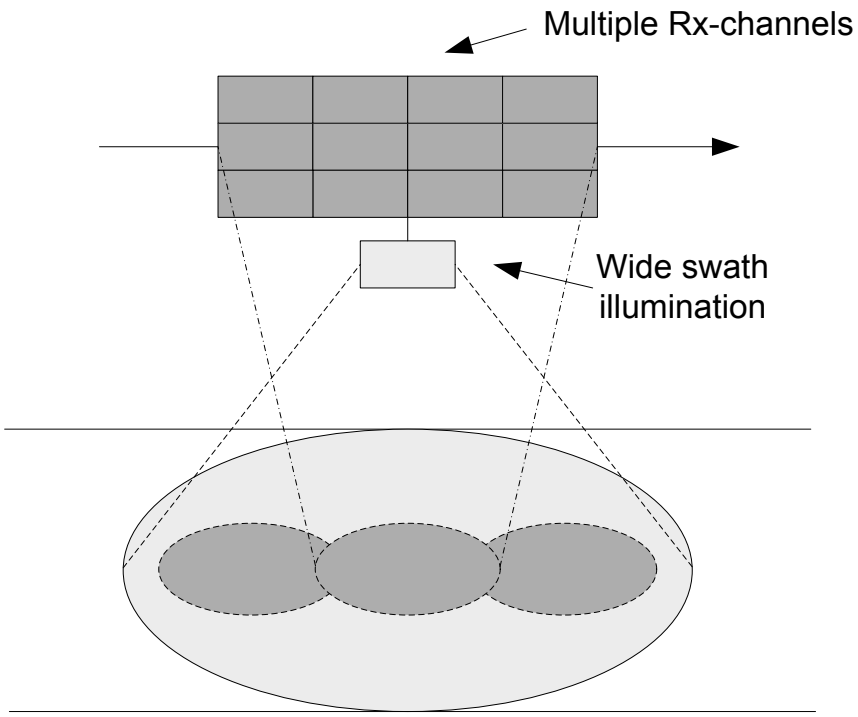

Figure 10: High-Resolution Wide-Swath SAR Simultaneously Improves Azimuth Resolution and Swath Width at Expenses of Hardware and Computational Complexity.

This imaging mode is only made possible due to the more recent technological advances that allow for digital beamforming techniques implementation with simultaneous multi-aperture signal acquisition. is currently under development and implementation at EADS Astrium, being supported by the German Aerospace Center (DLR) [13].

4.0 FINAL REMARKS

This paper is presents and discusses some of the most popular SAR geometries and imaging algorithms. In particular, the strip-map geometry – one of the most widely used SAR data acquisition techniques – was analysed. Firstly, a simple technique for SAR imaging, based on the possibility of processing range and cross-range dimensions separately, was presented. Although it is an approximation it permits focusing SAR images with sufficient quality for less demanding applications.

The framework of the wavefront reconstruction algorithm was then introduced. This algorithm is able to deal with the coupling between fast-time and slow-time domains tackling very accurately and efficiently the SAR inversion problem. It permits very high resolution imaging even in spaceborne applications.

Besides strip-map SAR, other popular SAR imaging modes were addressed. There is a trade-off limitation between resolution in azimuth versus spatial coverage when considering strip-map SAR, ScanSAR, or Spotlight SAR. To overcome this limitation the more advanced high-resolution wide-swath imaging SAR, was briefly described. It combines digital beamforming with multiple aperture recording in azimuth, enabling imaging of wide swath while simultaneously achieving high resolution.

5.0 ACKNOWLEDGEMENTS

The author wishes to acknowledge Prof. José-Bioucas Dias for the joint research activity carried together along several years that resulted in some of the publications and techniques that are herein summarized.

6.0 REFERENCES

[1] M. Soumekh, Fourier Array Imaging. Prentice Hall, 1994.

[2] A. Rihaczec, Principles of High-Resolution Radar. Artech House, 1996.

[3] M. Soumekh, Synthetic Aperture Radar Signal Processing with MATLAB algorithms. WILEY-INTERSCIENCE, 1999.

[4] D. C. Munson; R. L. Visentin, A signal processing view of strip-mapping synthetic aperture radar, IEEE transactions on Acoustics, Speech, and Signal Processing, Vol. 37, Issue 12, pp. 2131-2147, 1987.

[5] P. Marques, Moving objects imaging and trajectory estimation using a single synthetic aperture radar sensor, Ph.D. dissertation, Technical University of Lisbon, 2004.

[6] J. Bioucas-Dias, P. Marques, Multiple moving target detection and trajectory estimation using a single SAR sensor, IEEE Transactions on Aerospace and Electronic Systems, Vol. 39, No. 2, pp. 604-624, April 2003.

[7] J. Gazdag and P. Sguazzero, Migration of seismic data, Proceedings of the IEEE, Vol. 1, pp. 23-48, 1984.

[8] P. Gough and D. Hawkins, Imaging algorithms for a stripmap synthetic aperture sonar: Minimizing the effects of aperture errors and aperture undersampling, IEEE Journal of Oceanic Engineering, Vol. 22, No. 1, pp. 27-39, 1997.

[9] R. Raney, H. Runge, R. Bamler, I. Cumming, and F. Wong, Precision SAR processing using chirp scaling, IEEE Transactions on Geoscience and Remote Sensing, Vol. 32, No. 4, pp. 786-799, 1994.

[10] G. D. Callaghan and I. Longstaff, *"*Wide-swath space-borne SAR using a quad-element array,*"* IEE Proc. Radar, Sonar Navigation, Vol. 146, No. 3, pp. 155-165, 1999.

[11] C. Cafforio, C. Prati, and F. Rocca, *"*SAR data focusing using sysmic migration techniques,*"* IEEE Transactions on Aerospace and Electronic Systems, Vol. 27, No. 2, pp. 194-206, March 1991.

[12] H. Stolt, *"*Migration by Fourier transform,*"* Geophysics, Vol. 1, pp. 23-48, February 1978.

[13] A. Moreira, *"*A golden age for spaceborne SAR systems*"*, International Conference on Microwaves, Radar, and Wireless Communication, MIKON, 2014.